ACS APPLIED MATERIALS & INTERFACES

Research Article

www.acsami.org

One-Pot Synthesis of Water-Swellable Mg–Al Layered Double Hydroxides and Graphene Oxide Nanocomposites for Efficient Removal of As(V) from Aqueous Solutions

Tao Wen,[†,‡] Xilin Wu,[§] Xiaoli Tan,[†] Xiangke Wang,*[,†,‡] and Anwu Xu*[,∥]

[†]Key Laboratory of Novel Thin Film Solar Cells, Institute of Plasma Physics, Chinese Academy of Sciences, P.O. Box 1126, 230031, Hefei, P.R. China

[‡]School for Radiological and Interdisciplinary Sciences (RAD-X), Medical College of Soochow University, Suzhou 215123, PR China

[§]College of Nuclear Science and Technology and [∥]Division of Nanomaterials and Chemistry, Hefei National Laboratory for Physical Sciences at Microscale Department, University of Science and Technology of China, Hefei, 230026, P.R. China

Supporting Information

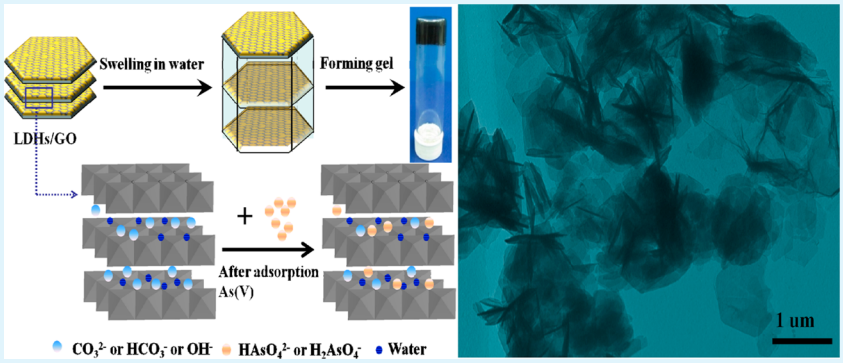

ABSTRACT: In this Article, we report a remarkably simple and efficient method for the preparation of layered double hydroxides and graphene oxide (LDHs/GO) nanocomposites with varying GO amounts via a hydrothermal process. The graphene nature in the resulting LDHs/GO nanocomposites was confirmed by X-ray diffraction (XRD), Fourier transformed infrared (FTIR) spectroscopy, field-emission scanning electron microscopy (FE-SEM), transmission electron microscopy (TEM), N_2 adsorption-desorption, and X-ray photoelectron spectroscopy (XPS). The LDHs/GO nanocomposites exhibited swelling behavior in water and forming a gel. The adsorption performance of the LDHs/GO nanocomposites was evaluated for the removal of arsenate (As(V)) from aqueous solutions, and the results showed that the ratio of GO to LDHs in the nanocomposites significantly affected the adsorption capacity. Higher and lower amounts of GO in LDHs/GO nanocomposites showed lower adsorption capacity of As(V). A maximum adsorption capacity of 183.11 mg/g (2.44 mmol/g) was achieved on the LDHs/GO containing 6.0% GO due to the higher Brunauer–Emmett–Teller (BET) surface area than other samples. Owing to their high uptake capability of As(V), water-swellable LDHs/GO nanocomposites are expected to have potential applications as adsorbents for As(V) polluted water cleanup.

KEYWORDS: *layered double hydroxides/graphene oxide, nanocomposites, As(V), adsorption*

1. INTRODUCTION

Widespread contamination of freshwater systems has become one of the forefront environmental problems. Among all water contaminants, arsenic has been known as one of the most toxic substances and carcinogenic chemical elements for centuries. Arsenic contamination is not only caused by natural processes such as mineral weathering and dissolution of metal oxide deposits but also generated by human activities such as agricultural chemicals and ceramic manufacturing industries.[1] Various techniques have been applied to remove As(V) from wastewater. Compared to other conventional techniques such as coagulation,[2] filtration,[3] oxidation,[4] reverse osmosis,[5] and biological treatment,[6] adsorption is considered as one of the most promising technologies owing to its cost-effective, versatile, and operational simplicity for removing trace levels of As(V) anions. To meet the fast-developing water treatment requirements, there is great need to devise new and innovative technologies and materials for efficient removal of As(V) from aqueous solutions.

Recently, graphene-based materials such as graphene and chemical modified graphene including graphene oxide (GO) have attracted considerable attention owing to their remarkable

Received: January 26, 2013
Accepted: March 25, 2013
Published: March 25, 2013

enhanced adsorption and multifunctional properties. For example, Zhao et al.[7] reported that highly dispersed sulfonated graphene nanosheets showed very high adsorption capacities for the removal of naphthalene and 1-naphthol from aqueous solutions. Chandra and Kim[8] fabricated polypyrrole−reduced graphene oxide composites with high selectivity for Hg^{2+} removal from aqueous solutions. Chandra et al.[9] synthesized magnetic-graphene hybrids showing high binding capacity for As(III) and As(V), resulting the complete arsenic removal within 1 ppb. Zhang et al.[10] found that ordered porous chitosan−gelatin/graphene oxide monoliths had excellent adsorption capacity for heavy metal ions such as Cu^{2+} and Pb^{2+} ions. The development of nanomaterials has acquired great significance in recent years due to their high efficiency and fast rates on water treatment. However, the study of graphene-based nanocomposites for wastewater treatment is still in the early stage.

Graphene is usually considered to be nonpolar and hydrophobic. GO contains much more polar moieties such as epoxy (C−O−C), hydroxyl (OH), and carboxy groups (COOH) on both basal planes and edges.[11,12] These functional groups are essential for the efficient adsorption of heavy metal ions. Layered double hydroxides (LDHs) are important inorganic layered materials with the generic formula $[M^{II}_{1-x}M^{III}_{x}(OH)_2]^{x+}(A^{n-})_{x/n}\cdot mH_2O$, where M^{II} and M^{III} are divalent and trivalent metal ions in the octahedral positions of brucite-like layers yielding excessive positive charge and A^{n-} represents a non-framework inorganic or organic *n*-valent anion compensating the interlayer anions related to hydrotalcite. The exchangeable interlayer anions of LDHs, incorporating a variety of anions, make them excellent adsorbents in water cleanup. Herein, the parent material of these anionic clays is the naturally occurring mineral hydrotalcite which has the formula $Mg_6Al_2(OH)_{16}CO_3\cdot 4H_2O$. Generally, most of the pure LDHs were prepared from conventional coprecipitation methods,[13−17] which could not increase their adsorption sites. However, graphene-based materials demonstrate several unique characteristics such as large surface area and potentially high binding energy. A recent study[9] reported that magnetite-graphene hybrids exhibited a high binding capacity for arsenic due to the increased adsorption sites. Thus, utilizing a strategy of fabricating nanocomposites by assembling the positively charged LDHs and carboxylated GO for the application of wastewater treatment would be of significance.

In this study, we reported a facile and environmentally friendly method for the synthesis of high-efficiency nano-adsorbents with high adsorption capacity for As(V). The large surface area of GO and the exfoliation of LDHs motivated us to synthesize LDHs/GO nanocomposites for As(V) adsorption. On the basis of this idea, we synthesized a series of LDHs/GO nanocomposites by varying the (w/w) ratio of 1.0%, 6.0%, and 11.0% of GO, denoted as LDHs/GO1, LDHs/GO2, and LDHs/GO3, respectively. The resulting assembly of LDHs/GO nanocomposites were observed for swelling in water leading to gel formation. The prepared LDHs/GO2 nanocomposites showed a practical approach for arsenic removal from water and a possible adsorption mechanism was proposed.

2. EXPERIMENTAL SECTION

2.1. Materials. Graphite powder (99.9995%, 325 mesh) was purchased from Alfa Aesar (Ward Hill, MA). $NaNO_3$, 98% H_2SO_4, $KMnO_4$, 30% H_2O_2, $MgCl_2\cdot 6H_2O$, $AlCl_3\cdot 6H_2O$, hexamethylene tetramine (HMT), NaOH, and 68% HNO_3 were obtained from Sinopharm Chemical Reagent Co., Ltd. All chemicals were of analytical grade and used without further purification. Milli-Q water (18.2 M Ω cm^{-1}) was used throughout the experiments.

2.2. Synthesis of LDHs/GO Nanocomposites. GO was synthesized using a modified Hummers method.[18,19] Generally, 3.0 g of graphite powder was preoxidized in 12 mL of concentrated H_2SO_4 containing 2.5 g of P_2O_5 and 2.5 g of $K_2S_2O_8$ at 80 °C for 4.5 h. Then, the mixture was diluted with 500 mL of water and filtered through a 0.22 μm Millipore nylon membrane. The product was rinsed with Milli-Q water and dried under room temperature. The preoxidized graphite and 120 mL of concentrated H_2SO_4 were mixed and stirred in a three-neck flask, and then 15 g of $KMnO_4$ was slowly added into the mixture under stirring with an ice bath. Once added, the solution was transferred to a 35 °C water bath and stirred for about 2 h, and then 250 mL of Milli-Q water was added with an ice-bath to keep the temperature below 50 °C. Then, the mixture was stirred for another 2 h and diluted with 700 mL of Milli-Q water, and 20 mL H_2O_2 (30%, v/v) was immediately added, turning the color of the solution from dark brown to yellow. The warm solution was filtered and rinsed thoroughly with HCl (1:10, v/v) and Milli-Q water. The filter cake was vacuum dried, and a dark brown GO powder was obtained.

The LDHs/GO samples with different GO compositions were synthesized through an alkaline hydrothermal treatment. First, (w/w) ratios of 1.0%, 6.0%, and 11.0% GO were ultrasonicated in 20 mL of Milli-Q water for 1 h to achieve homogeneous suspensions. Then, 20 mL of $MgCl_2-AlCl_3$−HMT solution containing 7.8 mmol $MgCl_2\cdot 6H_2O$, 2.6 mmol $AlCl_3\cdot 6H_2O$, and 9.2 mmol HMT was added to the above suspension. The resulting suspensions were stirred for 30 min and then transferred to a 50 mL Teflon-lined stainless-steel autoclave. The autoclave was heated to 140 °C and maintained for 12 h, and then cooled to room temperature. The resultant black slurry was centrifuged, washed with Milli-Q water, and vacuum dried at 60 °C overnight. Pure LDH nanoplates were made by the aforementioned procedure for comparison without any GO added.

2.3. Characterization. X-ray diffraction (XRD) patterns were collected using a Philips X'Pert Pro Super X-ray diffractometer with Cu Kα radiation (λ = 1.54178 Å). N_2 adsorption−desorption isotherms were performed with a Micromeritics ASAP 2010 system at 77 K utilizing Barrett−Emmett−Teller (BET) for specific surface area calculation. X-ray photoelectron spectroscopy (XPS) measurements were performed in a VG Scientific ESCALAB Mark II spectrometer equipped with two ultrahigh vacuum (UHV) chambers. Fourier transformed infrared (FTIR) spectra were recorded on a Nicolet Magana-IR 750 spectrometer over a range from 400 to 4000 cm^{-1}. Scanning electron microscopy (SEM) images were achieved using a JEOL JSM-6330F instrument operated at a beam energy of 15.0 kV. Transmission electron microscopic (TEM) images were acquired on a JEOL-2010 microscope. The zeta-potential was measured by using a ZETASIZER 3000 HSA system.

2.4. Adsorption Experiments. Batch adsorption experiments of arsenate on LDHs and LDHs/GO were carried out at pH 5.0 ± 0.1 and in 0.01 M $NaNO_3$ solutions in polyethylene test tubes. Stock suspensions were prepared by ultrasonication of 0.3 g of LDHs or LDHs/GO powders in Milli-Q water to achieve a concentration of 3.0 g L^{-1}. The stock suspension of LDHs/GO, As(V) solution, and $NaNO_3$ were added to 10 mL polyethylene test tubes to achieve the desired concentrations of different components. The desired pH of the suspensions in each tube was adjusted by adding negligible volumes of 0.01 or 0.1 M HNO_3 or NaOH solution. The results of kinetic adsorption suggested that As(V) adsorption on LDHs/GO achieved equilibrium in several hours. Therefore, after the mixture was oscillated for 24 h, the solid and liquid phases were separated by using 0.22 μm membrane filters. The concentration of As(V) in supernatant was determined with inductively coupled plasma mass spectrometry (ICP-MS). The amounts of As(V) adsorbed on LDHs or LDHs/GO were calculated from the difference between the initial concentration (C_0) and the equilibrium one (C_e):

$$\text{removal}\ (\%) = \frac{(C_0 - C_e)}{C_0} \times 100\% \quad (1)$$

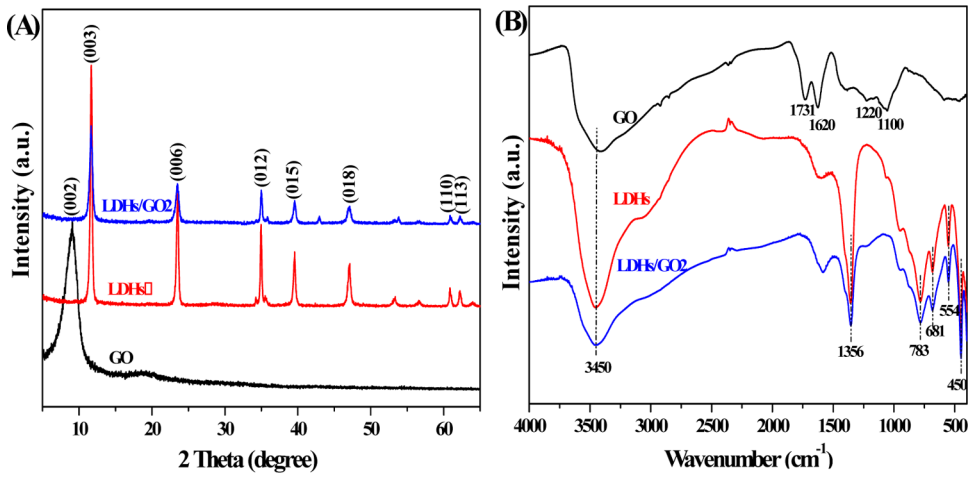

Figure 1. Characterization of as-prepared samples: (A) XRD patterns of GO, LDHs, and LDHs/GO2 samples; (B) FTIR spectra of GO, LDHs, and LDHs/GO2 samples.

$$q_e = \frac{(C_0 - C_e)}{m} V \quad (2)$$

where C_0 is the initial concentration (mg L^{-1}), C_e is the equilibrium concentration (mg L^{-1}), q_e is the amount of arsenate adsorbed on per weight of LDHs or LDHs/GO (mg g^{-1}), V is the volume of the suspension (L), and m is the mass of the adsorbent (g).

3. RESULTS AND DISCUSSION

3.1. Characterization of LDHs/GO2 Nanocomposites and Swelling Property. Figure 1A shows XRD patterns of GO, LDHs, and as synthesized LDHs/GO2 nanocomposites. The broad and strong diffraction peak at 2θ = 9.12°, corresponding to the typical diffraction peak of GO nanosheets, is attributed to the (002) plane of GO.[20] The peaks of LDHs at 2θ = 11.6° (003), 23.5° (006), 35.0° (012), 39.6° (015), 47.1° (018), 60.9° (110), and 62.3° (113) show the characteristics of Mg/Al LDH nanoplates.[21] It has to be noted that the as-prepared LDHs/GO2 is principally composed of a hexagonal LDHs phase and no diffraction peaks of impurities were discerned, indicating the high purity of the sample. Moreover, the features of the peaks are sharp and symmetric, suggesting that the as-prepared LDHs/GO2 was highly crystallized. The disappearance peak of GO at 2θ = 9.12° may be attributed to the very low content of GO in the nanocomposites. Based on the (003) reflection, one can determine the interlayer distance of LDHs/GO2 as ~7.58 Å. The results of the XRD analysis demonstrate that the LDHs/GO2 nanocomposites show good crystallinity and are successfully synthesized.

The FTIR spectra of GO, LDHs and LDHs/GO2 are given in Figure 1B. The strong peak at 3450 cm^{-1} is attributed to the stretching of O−H groups associated with the interlayer water molecules and hydrogen bonding. The strong peak at 1356 cm^{-1} was attributed to the vibration mode of CO_3^{2-} ions in the interlayer of Mg−Al LDHs. The bands in the range of 500−800 cm^{-1} are attributed to M−O, O−M−O, and M−O−M lattice vibrations (M = Mg and Al). Different functional groups are found in the FTIR spectrum of GO, that is, C═O group at 1731 cm^{-1} and C═C at 1620 cm^{-1}, C−O group at 1220 cm^{-1} and 1100 cm^{-1}, indicating the existence of large amounts of oxygen-containing functional groups on GO nanosheets.[22] The peaks in the spectrum of LDHs are consistent with those of LDHs/GO2, indicating the formation of LDHs/GO2 nanocomposites.

The morphology and microstructure of as-prepared LDHs/GO2 were characterized by SEM and TEM images. From the SEM images, one can see that the LDH/GO2 nanoplates were well dispersed on a copper grid (Figure 2c), whereas the pure

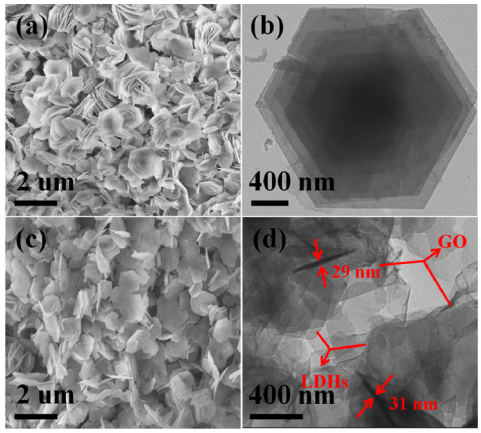

Figure 2. SEM images of LDHs (a) and LDHs/GO2 (c); TEM images of LDHs (b) and LDHs/GO2 (d).

LDHs were found to stack together in some areas (Figure 2a). As can be seen from the TEM images of LDHs (Figure 2b) and LDHs/GO2 (Figure 2d), the sample consisted of hexagonal platelets with the size about 1−2 μm, and their thickness was ≤40 nm. From the TEM image of LDHs/GO2, one can see that the wrinkled GO is firmly attached on the surface of the LDH nanoplates, indicating the formation of LDHs/GO2 nanocomposites. Evidently, the hydrothermal prepared LDHs/GO2 was of high quality in terms of hexagonal platelike morphology, size, and crystallinity, which could be attributed to a homogeneous and slow nucleation process owing to the slow hydrolysis of HMT. The LDHs/GO2 nanocomposites are found stable when subjected to stirring or ultrasound treatment, indicating that the positively charged LDHs are successfully grown on the surface of GO nanosheets by electrostatic interaction. The N_2−BET specific surface area of LDHs/GO2 (35.4 m^2/g) (see the Supporting Information, Figure S1A) is enhanced through the incorporation of LDHs and GO compared with that of LDHs (22.3 m^2/g). The LDHs/GO nanoplates also have a narrow pore size distribution centered at

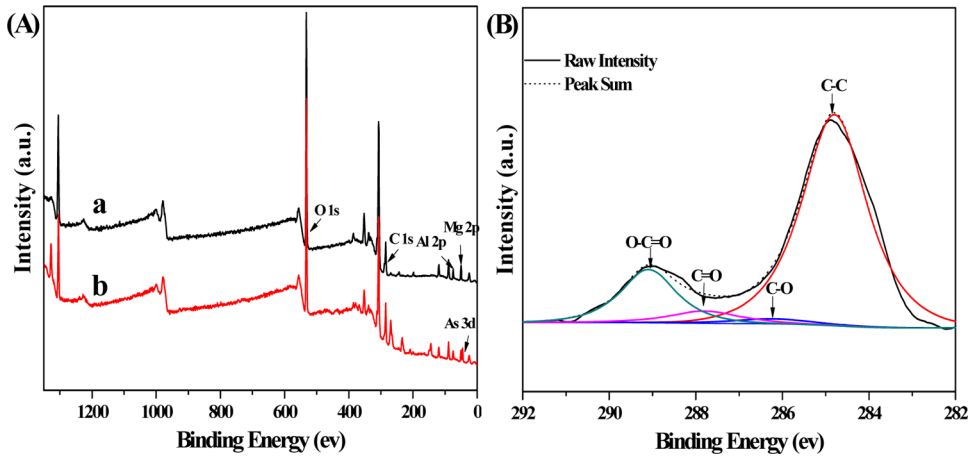

Figure 3. (A) XPS spectra of LDHs/GO2 survey: before (a) and after (b) As(V) adsorption. (B) XPS C 1s spectrum of LDHs/GO2.

3.9 nm, calculated from the desorption branch by the Barrett−Joyner−Halenda (BJH) method (see the Supporting Information, Figure S1B). Thus, the LDHs/GO2 nanocomposites can provide more active sites for As(V) uptake.

X-ray photoelectron spectroscopy (XPS) was further conducted to elucidate the surface state of the as-prepared and As(V)-adsorbed LDHs/GO2 nanocomposites (Figure 3A). Figure 3A shows the two survey spectra of LDHs/GO2 before and after As(V) adsorption. The XPS spectra reveal that oxygen, aluminum, and magnesium are the predominant elements observed on the surface from binding energy (E_B) values of O1s, Al2p, and Mg2p before adsorption. In contrast to the survey spectra of the as-prepared LDHs/GO2, the As(V) peak was observed in As(V)-adsorbed LDHs/GO2 (see the Supporting Information, summarized in Table S1), indicating an alteration of the local bonding environments occurred. Likely, it is ascribed to the specific adsorption of As(V) onto the surfaces of LDHs/GO2.[23] The C 1s XPS spectrum of LDHs/GO2 is shown in Figure 3B. The region of the spectrum can be deconvoluted into four components: the non-oxygenated ring C (284.8 eV), the carbon in C−O (286.2 eV), the carbonyl carbon (C═O, 287.9 eV), and the carboxylate carbon (O−C═O, 289.0 eV).[9] The specific peak area noted in Figure 3B shows that the main oxygen-containing group is O−C═O, which may be attributed to the intercalated CO_3^{2-} at the LDH phase that enhances the carboxylate carbon signal.

The swelling behavior of LDHs/GO2 in water was also conducted at room temperature. At lower volume fractions of LDHs/GO2, a clear transparent colloidal solution was obtained (Figure 4A). When a red laser beam was incident, a clear Tyndall light scattering was observed from the solution, indicating the presence of exfoliated LDHs/GO2 nanoplates dispersed in water (Figure 4B). The resulting colloidal suspension was very stable, and no sediment was observed on storing for 3 days. With increasing volume fraction of LDHs/GO2 solid dispersed in water, a stable gel, as characterized by the test tube inversion test, was obtained (Figure 4C). When LDH layers based on a carboxylated GO was synthesized via one-step hydrothermal method, the strong electrostatic force between the single-layer LDHs and GO facilitated the layered assembling of the two nanosheets.[24] The resulting swollen structure might be maintained by the strong electrostatic attractions between LDHs/GO2 layers and the guest anions as well as the weak H-bonding between water and LDHs/GO2 layers.[25] On the basis of the above results, it can be safely

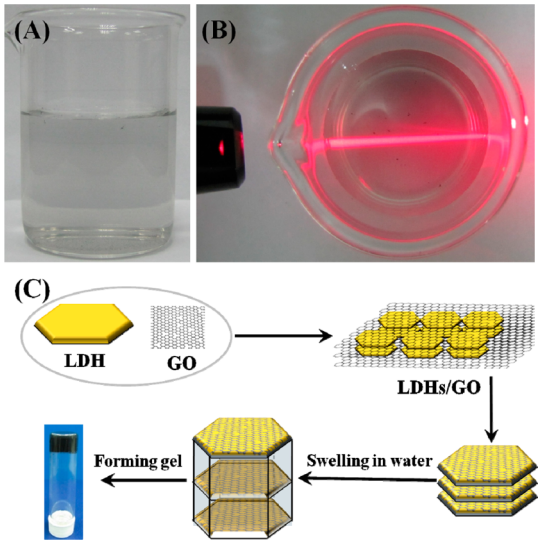

Figure 4. (A) Photograph of a dispersion of LDHs/GO2 nanoplates. (B) A red laser beam through the dispersions from the side to demonstrate the Tyndall effect. (C) Schematic illustration of the possible swelling behavior in water and photograph of LDHs/GO2 gel.

concluded that LDHs/GO2 swelled and immediately formed viscous gels on contact with water (about 6 times in weight), which are depicted schematically in Figure 4C.

3.2. Kinetics Study of As(V) Adsorption on LDHs/GO2.

Kinetics adsorption of As(V) on LDHs/GO2 was investigated in the presence of 0.5 g L^{-1} of adsorbent. Figure 5A shows that the adsorption rates were considerably fast in the first contact time of 2.5 h, and no significant change was observed from 2.5 to 24 h. This phenomenon that the adsorption reached equilibrium quickly indicated that the adsorption of As(V) on LDHs/GO2 was mainly attributed to chemical sorption or surface complexation. The binding of As(V) anions on the surface of LDHs/GO2 may be ascribed to the strong electrostatic interaction between As(V) and LDHs/GO2 layered structure. The other mechanism for arsenate adsorption is due to ion exchange between the intercalated anions of LDHs with As(V) anions. In addition, GO may provide extra adsorption sites for arsenate adsorption.

The experimental data were modeled by the pseudo-second-order rate equation. The pseudo-second-order rate constants (k_2) and the amount of As(V) adsorbed at equilibrium (q_e)

dx.doi.org/10.1021/am4003556 | ACS Appl. Mater. Interfaces 2013, 5, 3304−3311

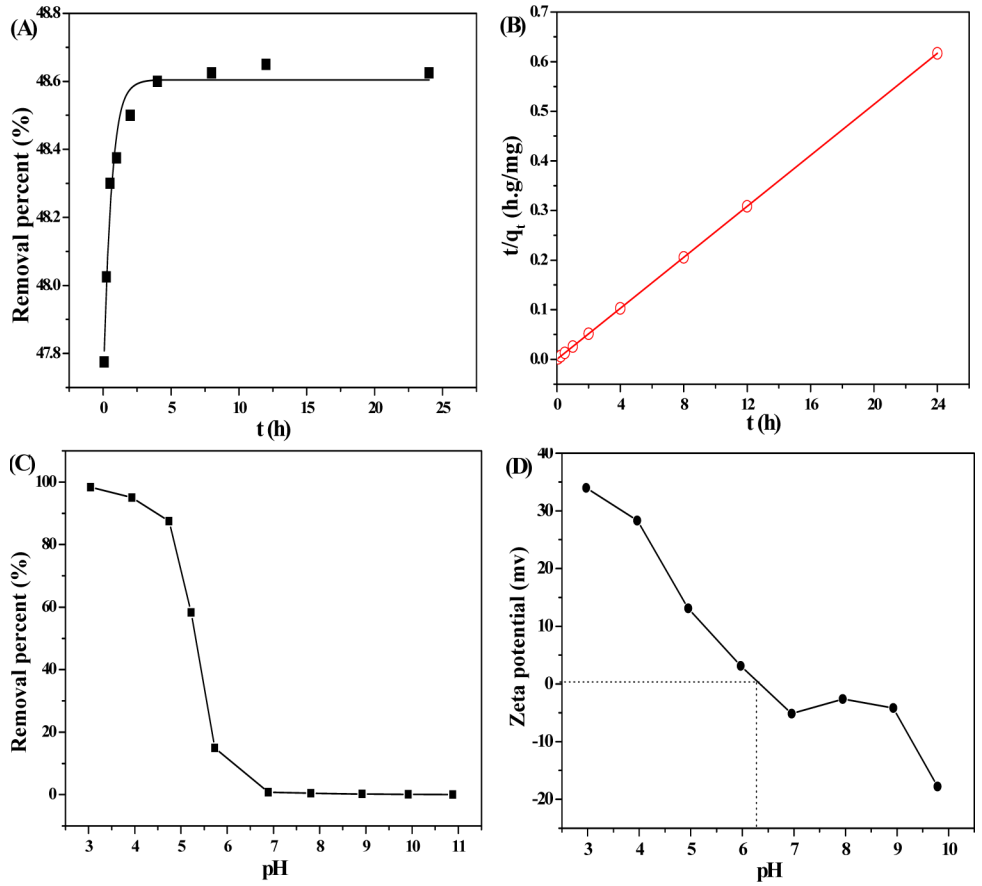

Figure 5. (A) Time profile of As(V) adsorption on LDHs/GO2 and (B) pseudo-second-order kinetic plots of t/q_t vs t. The initial concentration of As(V) is 40 mg L^{-1}, pH = 5.0 ± 0.1. (C) Effect of solution pH on the adsorption of As(V) by LDHs/GO2. (D) Zeta-potential of LDHs/GO2 as a function of pH. All batch adsorption experiments were conducted in m/V = 0.5 g L^{-1}, and I = 0.01 M $NaNO_3$ polyethylene test tubes.

were calculated from the intercept and slope of the plot of t/q_t vs t according to eq 3:[26]

$$\frac{t}{q_t} = \frac{1}{k_2 q_e^{\,2}} + \frac{t}{q_e} \qquad (3)$$

where q_t (mg g^{-1}) is the amount of arsenate at contact time t (h), q_e (mg g^{-1}) is the amount of arsenate adsorbed at equilibrium time, and k_2 (g mg^{-1} h^{-1}) is the pseudo-second-order rate constant. The kinetics of the adsorption process was shown in Figure 5B. The value of q_e calculated from the slope and intercept of the plot of t/q_t versus t is 38.91 mg g^{-1}, which is consistent with the experimental data (38.90 mg g^{-1}). The calculated q_e value was very close to the theoretical ones, showing quite good linearity with R^2 above 0.999. Therefore, the kinetic adsorption of As(V) on LDHs/GO2 follows the pseudo-second-order model, suggesting a chemisorption process.[27]

3.3. Effect of Solution pH on As(V) Adsorption. Effect of solution pH on As(V) uptake was conducted to test the effectiveness of LDHs/GO2 over a range of pH (Figure 5C). The adsorption percentage is high at low pH and decreases with increasing pH. The results showed that As(V) adsorption decreased gradually with increasing pH in the range of 3.0−4.7, where more than 80% of As(V) was removed from aqueous solution by LDHs/GO2. The As(V) adsorption on LDHs/GO2, however, decreased remarkably from ∼80% to ∼10% when solution pH increased from 4.7 to 6.0. The quite low adsorption percentage of As(V) was observed at pH > 6.0. To further understand the influence of pH on As(V) adsorption, the zeta-potential values of LDHs/GO2 were measured at different pHs, and the results are shown in Figure 5D. As can be seen, the electrostatic point of LDHs/GO2 was about 6.3. The surface charge of LDHs/GO2 might carry positive charges at pH < 6.3, which is favorable for the binding of negative charged As(V) anions, whereas at pH > 6.3, the surface charge of LDHs/GO2 becomes negative because of the deprotonation of the surface hydroxyl groups. Thus, the negative charged As(V) anions are difficult to be adsorbed on the negative charged surface of LDHs/GO2 because of electrostatic repulsion. With solution pH increasing, the concentration of OH^- increases, which can strongly compete with As(V) anions to enter into the interlayer of LDHs/GO2. Herein, the adsorption of As(V) anions on LDHs/GO2 is believed to occur via electrostatic interactions.[28]

3.4. Adsorption Isotherms and Mechanism. Due to the high specific surface area of GO and the exchangeable anions in the interlayers of LDHs, the resulting series of LDHs/GO were expected to probe the maximum adsorption capacity in the uptake of As(V) anions from aqueous solutions. Figure 6 shows the typical adsorption isotherms of As(V) on LDHs/GO nanocomposites with varying (w/w) ratios of 1.0%, 6.0%, and 11.0% of GO. The adsorption data were fitted with both Langmuir[29] and Freundlich[30] models described as follows:

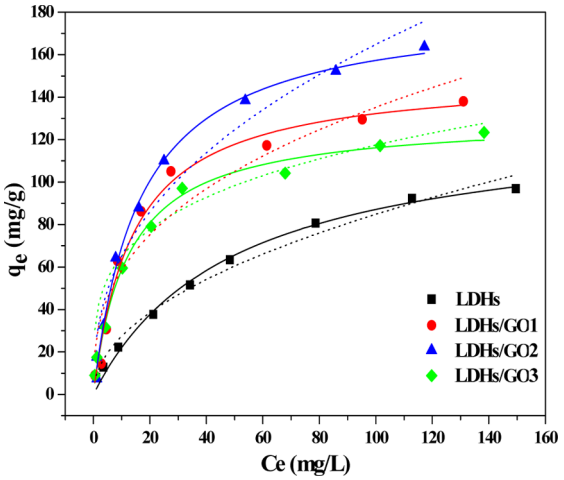

Figure 6. Adsorption isotherms of As(V) on LDHs, LDHs/GO1, LDHs/GO2, and LDHs/GO3. pH = 5.0 ± 0.1, m/V = 0.5 g L^{-1}, and I = 0.01 M $NaNO_3$. Symbols denote experimental data, solid lines represent the Langmuir model simulation, and dashed lines represent the Freundlich model.

Langmuir model:

$$q_e = \frac{bq_{max}C_e}{1 + bC_e} \quad (4)$$

Freundlich model:

$$q_e = kC_e^{1/n} \quad (5)$$

where C_e (mg L^{-1}) and q_e (mg g^{-1}) are the equilibrium concentration of As(V) in the supernatant and the amount of As(V) adsorbed on per weight of LDHs/GO at equilibrium, respectively. q_{max} (mg g^{-1}) is the maximum adsorption capacity associated with complete monolayer coverage, and b (L mg^{-1}) is a Langmuir constant related to the energy and affinity of the sorbent. The Freundlich constant k is correlated to the relative adsorption capacity of the adsorbent (mg g^{-1}), and n is related to the energetic heterogeneity (average energy of sites). The N_2–BET specific surface area, S_{BET}, and the values of the corresponding maximum adsorption capacity, q_{max}, relating to correlation coefficient and complete monolayer coverage are given in Table 1. The higher correlation coefficient of the Langmuir model indicates that the adsorption data are better fitted by the Langmuir model rather than by the Freundlich model. The binary LDHs/GO compositions with varying GO amounts showed enhanced As(V) adsorption capability as compared with the individual LDHs (129.71 mg/g) due to their higher specific surface area than LDHs. For comparison, the q_{max} values of As(V) on other different adsorbents are listed in Table 2. The highest adsorption capacity of 183.11 mg/g was achieved on LDHs/GO2 as compared with the previously investigated adsorbents such as magnetite-reduced graphene oxide (5.83 mg/g),[9] α-FeOOH (58 mg/g),[31] PANI modified active carbon (1.43 mg/g),[32] iron(III) oxide coated ethylenediamine modified MWCNTs (18.05 mg/g),[33] Zr(IV)-loaded orange waste gel (88.0 mg/g),[34] and chitosan-coated biosorbent (96.46 mg/g).[35] The LDHs/GO2 nanocomposites were found to possess a high adsorption capacity of As(V) owing to their exchangeable interlayer anions and perfect nanocrystalline property. It is necessary to note that all the n values of Freundlich constant are greater than 2, indicating that As(V) adsorption on all samples are favorable processes. Moreover, LDHs were hybridized with mechanically and chemically stable graphene-based materials through one-step hydrothermal reaction, providing an accessible diffusion pathway in the macropore domain.[36] We thus believe that LDHs/GO2 with exceptionally high adsorption capacities for As(V) is expected to have potential applications for practical water treatment.

Table 2. Comparison of the Maximum Adsorption Capacity of As on LDHs/GO with Other Different Adsorbents

adsorbents	pH	adsorption capacity (mg/g)	ref
polyaniline PANI modified active carbon	5.5	1.43	32
magnetite-reduced graphene oxide	7.0	5.83	9
iron(III) oxide coated ethylenediamine modified MWCNTs	4.0	18.05	33
α-FeOOH		58	31
Zr(IV)-loaded orange waste gel	3.0	88.0	34
chitosan-coated biosorbent	4.0	96.46	35
LDHs	5.0	129.71	this study
LDHs/GO2	5.0	180.26	this study

To further investigate the adsorption mechanism, As(V)-adsorbed LDHs/GO2 nanocomposites were firstly prepared. Figure 3A shows full-range XPS spectra of before and after As(V) adsorption, confirming that arsenate ions are adsorbed on the surface of LDHs/GO2. The high resolution XPS spectrum of As(V)-adsorbed sample (see the Supporting Information, Figure S2C) shows the characteristic binding energies associated with the As_{3d} photoelectron located at 45.39 eV.[37] As can be seen in Figure S2 in the Supporting Information, the high resolution C 1s spectrum of LDHs/GO2 shows a peak located at 288.4 eV, which can be assigned to the intercalated CO_3^{2-} at the LDH phase. The intensity of carbonate after As(V) adsorption (see the Supporting Information, Figure S2A and B), however, becomes significantly lower, reduced from ~24% to ~20%, indicating that the partial replacement of interlayer CO_3^{2-} were exchanged by

Table 1. S_{BET} = BET Specific Surface Area Obtained from N_2 Adsorption Data in the P/P_0 Range from 0.05 to 0.20; Summary of the Langmuir and Freundlich Isotherm Model Parameters for the As(V) Uptake Capacity on LDHs and LDHs/GO of Varying GO Content

		Langmuir			Freundlich		
sample name	S_{BET} (m^2/g)	q_{max} (mg g^{-1})	b (L mg^{-1})	R^2	k	n	R^2
LDHs	22.3	129.71	0.0206	0.992	8.86	2.04	0.984
LDHs/GO1	32.0	150.77	0.0714	0.984	25.24	2.78	0.904
LDHs/GO2	35.4	180.26	0.0618	0.992	25.33	2.50	0.951
LDHs/GO3	27.3	130.30	0.0819	0.992	35.98	3.85	0.917

dx.doi.org/10.1021/am4003556 | ACS Appl. Mater. Interfaces 2013, 5, 3304–3311

$HAsO_4^{2-}$ /$H_2AsO_4^-$. Furthermore, the FTIR spectrum (see the Supporting Information, Figure S3) of LDHs/GO2 after As(V) adsorption demonstrates that the intensity of carbonate and hydroxyl groups are much lower than that of LDHs/GO2 before adsorption, suggesting that both of carbonate and hydroxyl groups play roles in the removal process. Whereas Cao et al.[38] fabricated basic aluminum carbonate (Al(OH)-CO_3) and found that the adsorption mechanism was ion exchange between carbonate groups and As(V). Based on the above results, the adsorption mechanism of As(V) was illustrated in Figure 7. When dissolving the LDHs/GO in a

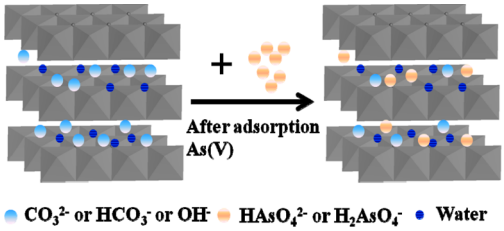

Figure 7. Schematic representation mechanism of As(V) adsorption onto LDHs/GO.

solution containing As(V), the uptake of As(V) was mainly via ion exchange in the interlayer of LDHs/GO, that is, the partial replacement of interlayer CO_3^{2-}/HCO_3^-/OH^- ions by arsenate ions.[15] The toxic As(V) ions can be quickly and efficiently removed in this way.[39]

4. CONCLUSIONS

In summary, water-swellable layered double hydroxides and graphene oxide nanocomposites (LDHs/GO) with varying GO amounts are fabricated using a simple one-pot hydrothermal method, and the LDHs were successfully grown on the surface of GO. The as-prepared LDHs/GO2 exhibited swelling behavior in water (about 6 times in weight) leading to the formation of gel, and As(V) adsorption onto the hybrid materials was investigated. The obtained LDHs/GO2 showed much higher adsorption capacity (183.11 mg/g) and excellent ability to remove As(V) from large volumes of aqueous solutions as compared with other materials. The adsorption isotherms can be well fitted by the Langmuir model which is indicative of a monolayer adsorption. The mainly adsorption mechanism may be attributed to ion exchange in the interlayer of LDHs/GO nanocomposites. From the results, the LDHs/GO nanocomposites are potential candidates for the application in wastewater purification.

■ ASSOCIATED CONTENT

Supporting Information

Additional figures and table as described in the text. This material is available free of charge via the Internet at http://pubs.acs.org.

■ AUTHOR INFORMATION

Corresponding Author

*E-mail: xkwang@ipp.ac.cn (X.K.W.); anwuxu@ustc.edu.cn (A.W.X.). Tel.: +86 -551-65592788. Fax: +86-551-65591310.

Notes

The authors declare no competing financial interest.

■ ACKNOWLEDGMENTS

Financial support from 973 projects (Grant No. 2011CB933700) and NSFC (Grant No. 21077107; 21225730) is acknowledged.

■ REFERENCES

(1) Manning, B. A.; Goldberg, S. *Environ. Sci. Technol.* **1997**, *31*, 2005.
(2) Song, S.; Lopez, V. A.; Hernandez, C. D. J.; Peng, C.; Monroy, F. M. G.; Razo, S. I. *Water Res.* **2006**, *40*, 364.
(3) Meng, X. G.; Korfiatis, G. P.; Christodoulatos, C.; Bang, S. *Water Res.* **2001**, *35*, 2805.
(4) Leupin, O. X.; Hug, S. J. *Water Res.* **2005**, *39*, 1729.
(5) Ning, R. Y. *Desalination* **2002**, *143*, 237.
(6) Ma, L. M.; Zhang, W. X. *Environ. Sci. Technol.* **2008**, *42*, 5384.
(7) Zhao, G. X.; Jiang, L.; He, Y. D; Li, J. X; Dong, H. L; Wang, X. K; Hu, W. P. *Adv. Mater.* **2011**, *23*, 3959.
(8) Chandra, V.; Kim, K. S. *Chem. Commun.* **2011**, *47*, 3942.
(9) Chandra, V.; Park, J.; Chun, Y.; Lee, J. W.; Hwang, I. C.; Kim, K. S. *ACS Nano* **2010**, *4*, 3979.
(10) Zhang, N. N.; Qiu, H. X.; Si, Y. M; Wang, W.; Gao, J. P. *Carbon* **2011**, *49*, 827.
(11) Compton, O. C.; Nguyen, S. T. *Small* **2010**, *6*, 711.
(12) Mei, Q. S.; Zhang, Z. P. *Angew. Chem. Int. Ed.* **2012**, *51*, 5602.
(13) Chetia, M.; Goswamee, R. L.; Banerjee, S.; Chatterjee, S.; Singh, L.; Srivastava, R. B.; Sarma, H. P. *Clean Technol. Environ. Policy* **2012**, *14*, 21.
(14) Violante, A.; Pucci, M.; Cozzolino, V.; Zhu, J.; Pigna, M. *J. Colloid Interface Sci.* **2009**, *333*, 63.
(15) Wang, S. L.; Liu, C. H.; Wang, M. K.; Chuang, Y. H.; Chiang, P. N. *Appl. Clay Sci.* **2009**, *43*, 79.
(16) Goh, K. H.; Lim, T. T.; Dong, Z. L. *Environ. Sci. Technol.* **2009**, *43*, 2537.
(17) Goh, K. H.; Lim, T. T.; Dong, Z. L. *Water Sci. Technol.* **2010**, *61*, 1411.
(18) Hummers, W. S.; Offeman, R. E. *J. Am. Chem. Soc.* **1958**, *80*, 1339.
(19) Xu, Y. X.; Bai, H.; Lu, G. W.; Li, C.; Shi, G. Q. *J. Am. Chem. Soc.* **2008**, *130*, 5856.
(20) Wang, H. L.; Robinson, J. T.; Li, X. L.; Dai, H. J. *J. Am. Chem. Soc.* **2009**, *131*, 9910.
(21) Xu, Z. P.; Lu, G. Q. *Chem. Mater.* **2005**, *17*, 1055.
(22) Zhao, G. X.; Li, J. X.; Ren, X. M.; Chen, C. L.; Wang, X. K. *Environ. Sci. Technol.* **2011**, *45*, 10454.
(23) Gong, J. M.; Liu, T.; Wang, X. Q.; Hu, X. L.; Zhang, L. Z. *Environ. Sci. Technol.* **2011**, *45*, 6181.
(24) Wang, L.; Wang, D.; Dong, X. Y.; Zhang, Z. J.; Pei, X. F.; Chen, X. J.; Chen, B.; Jin, J. *Chem. Commun.* **2011**, *47*, 3556.
(25) Liu, Z. P.; Ma, R. Z.; Osada, M.; Iyi, N.; Ebina, Y.; Takada, K.; Sasaki, T. *J. Am. Chem. Soc.* **2006**, *128*, 4872.
(26) Liu, M. C.; Chen, C. L.; Hu, J.; Wu, X. L.; Wang, X. K. *J. Phys. Chem. C* **2011**, *115*, 25234.
(27) Bhattacharya, A. K.; Naiya, T. K.; Mandal, S. N.; Das, S. K. *Chem. Eng. J.* **2008**, *137*, 529.
(28) Wang, L.; Wu, X. L.; Xu, W. H.; Huang, X. J.; Liu, J. H.; Xu, A. W. *ACS Appl. Mater. Interfaces* **2012**, *4*, 2686.
(29) Langmuir, I. *J. Am. Chem. Soc.* **1918**, *40*, 1361.
(30) Freundlich, H. M. F. *J. Phys. Electrochem.* **1906**, *57*, 385.
(31) Wang, B.; Wu, H. B.; Yu, L.; Xu, R.; Lim, T. T.; Lou, X. W. *Adv. Mater.* **2012**, *24*, 1111.
(32) Yang, L.; Wu, S.; Chen, J. P. *Ind. Eng. Chem. Res.* **2007**, *46*, 2133.
(33) Veličković, Z.; Vuković, G. D.; Marinković, A. D; Moldovan, M. S.; Perić-Grujić, A. A.; Uskoković, P. S.; Ristić, M. D. *Chem. Eng. J.* **2012**, *181–182*, 174.
(34) Biswas, B. K.; Inoue, J.; Inoue, K.; Ghimire, K. N.; Harada, H.; Ohto, K.; Kawakita, H. *J. Hazard. Mater.* **2008**, *154*, 1066.
(35) Boddu, V. M.; Abburi, K.; Talbott, J. L.; Smith, E. D.; Haasch, R. *Water Res.* **2008**, *42*, 633.

(36) Wu, X. L.; Wang, L.; Chen, C. L.; Xu, A. W.; Wang, X. K. *J. Mater. Chem.* **2011**, *21*, 17353.
(37) Bang, S.; Johnson, M. D.; Korfiatis, G. P.; Meng, X. G. *Water Res.* **2005**, *39*, 763.
(38) Cao, C.Y.; Li, P.; Qu, J.; Dou, Z. F.; Yan, W. S.; Zhu, J. F.; Wu, Z. Y.; Song, W. G. *J. Mater. Chem.* **2012**, *22*, 19898.
(39) Yu, X.Y.; Luo, T.; Jia, Y.; Xu, R. X.; Gao, C.; Zhang, Y. X.; Liu, J. H.; Huang, X. J. *Nanoscale* **2012**, *4*, 3466.